journal

J. Am. Ceram. Soc., 76 [1] 113–22 (1993)

Transformation Textures in Zirconia

Keith J. Bowman*

School of Materials Engineering, Purdue University, West Lafayette, Indiana 47907

I-W. Chen*

Department of Materials Science and Engineering, The University of Michigan, Ann Arbor, Michigan 48109

The large shear component of the tetragonal-to-monoclinic transformation in zirconia causes a stress-induced preferred orientation of the tetragonal and monoclinic variants. The resultant texture, which is dependent on the loading condition, has been analyzed in terms of stress assistance to transformation and experimentally verified in simple tension and compression. Such a preferred orientation is a clear indication of the shear contribution to transformation plasticity and to fracture. Other implications of this analysis are also explored. For example, while the monoclinic texture is obviously most relevant to generating strains and plastic work, it is the tetragonal texture which might be advantageously tailored to enhance transformability and toughness. Transformation texture causes the ratio of {111} monoclinic and tetragonal X-ray peaks in tensile fracture to be higher than the actual ratio of monoclinic-to-tetragonal phase fractions, making it generally unsuitable for estimating phase fraction in stress-induced transformation.

I. Introduction

TRANSFORMATION texture in the form of orientation relationships between parent and product phases is a common observation in phase transformation studies. Specifically, an initially textured parent phase will necessarily lead to a product phase with an inherited preferred orientation. Examples in metallurgy include martensitic transformation or austenite to ferrite transformation in rolled steels.[1,2] In geology, transformation from textured hematite is believed responsible for the textured magnetite deposits.[3] Transformation textures can also arise from a stress bias without any initial texture in the parent phase. Very few reports of the latter phenomenon are available in the metallurgy literature, however, because most metal products are already textured as a result of thermal–mechanical processing.[4–6]

In recent years, evidence has been accumulated for a strong transformation texture in zirconia-containing ceramics which undergo mechanically induced transformation.[7–18] Such evidence is readily available for the X-ray diffraction patterns reported for fractured or ground surfaces of zirconia specimens and is most commonly manifested by a highly distorted intensity profile of the tetragonal (parent) and monoclinic (product) phases. In addition, the observation of a macroscopic shear strain in transformation plasticity provides indirect evidence for transformation texture.[19,20] The present paper reports a theoretical and experimental study of transformation texture of zirconia under simple tension and compression conditions.

Texture from stress-biased transformation can be rationalized rather simply, using the concept of stress assistance for martensitic transformation.[19,20] Since certain variants in the parent tetragonal phase are more favorably oriented relative to the stress axis, they would transform to the monoclinic phase first, resulting in a texture of the remaining tetragonal phase. The monoclinic phase may also become textured if during transformation the lattice correspondence and variant that produce the largest transformation strain coupled to the applied stress are selected or if a particular monoclinic variant becomes predominant in mechanical twinning of the monoclinic phase. In a polycrystal, however, the above consideration is often complicated by autocatalysis of the transformation which may obliterate variant selection, the presence of internal stress which augments the applied stress, and the self-accommodation of the parent and product phases which causes twinning in the monoclinic variants.[11,16,19,20] On the other hand, since slip is not a viable room-temperature deformation mechanism in zirconia, transformation-induced macroscopic plastic deformation (i.e., transformation plasticity) must be entirely accounted for by the crystallographic orientation distributions of the parent and product phases at all stages. A quantitative texture analysis in the course of stress-assisted transformation thus offers an incisive tool to track the mechanisms operational in transformation plasticity. Finally, inasmuch as the tetragonal and monoclinic phases are invariably textured in case of mechanically induced transformation, the texture analysis also provides a rationalized basis for estimating phase fraction from X-ray intensity comparison, which is a commonly used technique in zirconia research. The present investigation was carried out with the above considerations in mind.

II. Stress Assistance and Variant Orientation Distribution

For transformation of a tetragonal crystal to a monoclinic crystal with a common c axis shared by the two phases (lattice correspondence C), the transformation strain e is given by

$$\begin{vmatrix} e_{11} & 0 & e_{13} \\ 0 & e_{22} & 0 \\ 0 & 0 & e_{33} \end{vmatrix} \quad \text{or} \quad \begin{vmatrix} e_{11} & 0 & 0 \\ 0 & e_{22} & e_{23} \\ 0 & 0 & e_{33} \end{vmatrix} \tag{1a}$$

Likewise, for the shared a axis (lattice correspondence A), the transformation strain is given by

$$\begin{vmatrix} e_{11} & 0 & 0 \\ 0 & e_{22} & 0 \\ e_{31} & 0 & e_{33} \end{vmatrix} \quad \text{or} \quad \begin{vmatrix} e_{11} & 0 & 0 \\ 0 & e_{22} & 0 \\ 0 & e_{32} & e_{33} \end{vmatrix} \tag{1b}$$

In the above, the magnitude of the shear term can be denoted by γ or $-\gamma$, the negative sign allowed because shear in either direction is equivalent. In all, then, there are eight equivalent choices of shear systems.

A. V. Virkar—contributing editor

Manuscript No. 196273. Received October 21, 1991; approved August 25, 1992.

Supported by the National Science Foundation under Grant Nos. DMR-8807024 and DMR 8819186.

*Member, American Ceramic Society.

For axisymmetric deformation under a uniaxial stress σ in the z direction, the axial strain in the same axis, e_{zz}, is of special interest, giving the external work W equal to σe_{zz}. The above work can be expressed as

$$W = \sigma(e_{11}\sin^2\alpha\cos^2\beta + e_{22}\sin^2\alpha\sin^2\beta + e_{33}\cos^2\alpha) + \left|\left(\frac{e_{13}+e_{31}}{2}\sin 2\alpha\cos\beta + \frac{e_{23}+e_{32}}{2}\sin 2\alpha\sin\beta\right)\right| \quad (2)$$

Here we refer to Fig. 1 and let α be the angle between the c axis and the stress axis z, and β be the angle between the b axis and the reference coordinate y axis, which lies on the a–b plane. In the above expression, only one shear component is nonzero, and it should be the one that gives the largest positive shear work among the eight equivalent shear systems. In this sense, the shear component of W is rather similar to the Schmid factor for slip deformation of a single crystal subject to the same loading condition. The above result has been derived by Chen and Reyes-Morel[19,20] previously but is shown here in a slightly different form to facilitate tensorial computation.

If transformation is dictated by the stress assistance consideration, then the selection of the tetragonal and monoclinic variants is determined by the magnitude of W alone. The macroscopic strain ε is then determined by summing all the crystallographic transformation strains

$$\varepsilon_{ij} = \frac{1}{n}\sum_{p=1}^{m} A_{ik}^{\{p\}}A_{jl}^{\{p\}}e_{kl} \quad (3)$$

where

$$A = \begin{pmatrix} \cos\alpha\cos\beta & \cos\alpha\sin\beta & -\sin\alpha \\ -\sin\beta & \cos\beta & 0 \\ \sin\alpha\cos\beta & \sin\alpha\sin\beta & \cos\alpha \end{pmatrix} \quad (4)$$

as determined from the directional cosines between (xyz) and (abc) coordinates. In the above expression, p is an index for the m transforming tetragonal grains, among a total of n available tetragonal grains. The fraction of transformation is simply m/n.

Let us now evaluate W for some extreme cases. We will choose the following transformation strain for lattice correspondence C

$$\begin{vmatrix} 0 & 0 & \pm 0.16 \\ 0 & 0.025 & 0 \\ 0 & 0 & 0.25 \end{vmatrix} \quad \text{or} \quad \begin{vmatrix} 0.025 & 0 & 0 \\ 0 & 0 & \pm 0.16 \\ 0 & 0 & 0.025 \end{vmatrix} \quad (5)$$

(The case for lattice correspondence A is similar.) The maximum value of Eq. (2), W_{max}, is approximately $0.07\,|\sigma|$ in compression (for a maximum compressive axial strain -0.07), for a grain with orientation $\alpha \approx 40°$ and $\beta = 0$. In tension, the maximum value is 0.09σ (for a maximum tensile axial strain 0.09) for a grain with orientation $\alpha \approx 50°$ and $\beta = 0°$. These grains are the ones that produce the largest resolved axial strains along the stress axis. If stress assistance is the only criterion for transformation, then the transformation will start from these grains and proceed to others which produce progressively less resolved axial strains. Note that the slight difference between tension and compression is caused by dilatational transformation strains e_{11}, e_{22}, and e_{33}. Without them, the most favorable transformation orientations would be those with $\alpha = 45°$ and $\beta = 0°$, and the strain would be ± 0.08 in tension and compression.

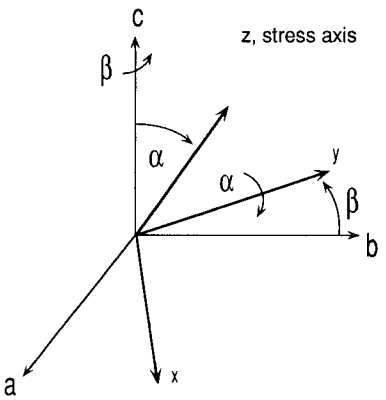

Fig. 1. Tetragonal crystal (a,b,c), the specimen coordinate (x,y,z) and Euler angles α and β. Note that y is on (a,b) plane.

We can survey all the solid angles of the tetragonal grains to determine their corresponding resolved strains and hence the stress assistance during transformation, assuming that the most favorable monoclinic variants for either lattice correspondence C or A always follow. Shown in Fig. 2 are strain (or stress assistance) contours normalized by the maximum axial strain (or stress assistance) in an equal-area projection expressed in the orientation of the tetragonal crystal with respect to the stress axis. A slight difference in tension and in compression due to the nonpure shear component is again evident. In particular, in compression, a small fraction of tetragonal phase (shown as the shaded areas in Fig. 2) produces no resolved compressive axial strain along the stress axis and thus receives no stress assistance. This is so because of the dilatational component of transformation strain. No such case is encountered in tension.

The fraction of grains for a particular stress assistance or strain can be evaluated by counting the number of grains in the entire span of solid angles within the contour map of Fig. 2. Shown in Fig. 3 is the cumulative fraction of tetragonal grains that receive a certain stress assistance. From the plot we can estimate that in tension 50% of tetragonal grains receive stress assistance of 0.063σ or more, while in compression the corresponding value is only $0.040\,|\sigma|$. This difference is caused not only by the different distributions as shown in Fig. 2, but also by the different W_{max} in tension and in compression.

The transformation stereograms of Fig. 2 can be readily transformed into the standard form of pole figure. However, standard pole figure representation requires an internal normalization which keeps the number of certain poles within a material constant. This normalization is used to relate reorientations of poles in conventional textures. For transformation textures the phase fractions change, which means that poles of a particular type will change in a number of ways, including orientation, multiplicity, and structure factor. For this reason, pole distributions, calibrated to the fraction of poles, are employed in this work and are used for comparisons with experimentally measured intensities of corresponding poles. For a tetragonal material, a pole fraction of magnitude one represents the initial number of poles present within the material. The corresponding pole fraction for transformation to a monoclinic material represents the number of poles present of a certain type at a particular orientation after transformation. The reduction in symmetry for tetragonal-to-monoclinic transformation causes a bifurcation in the poles for most types. A pole distribution can be produced by calculating the fraction of a random set of tetragonal grain orientations with $\{hkl\}$ normals parallel to specimen orientations. As these tetragonal grains transform, the pole distribution will evolve systematically as a function of the angle from the stress axis. Details of the calculation used to generate the transformation pole distributions are given in the Appendix. Examples of such pole distributions for several tetragonal reflections are given below.

III. Pole Distributions of Tetragonal and Monoclinic Reflections

Pole distribution as used here refers to the intensity of a particular reflection peak (pole) plotted against specimen orientation. In our case, the orientation is defined with respect to the

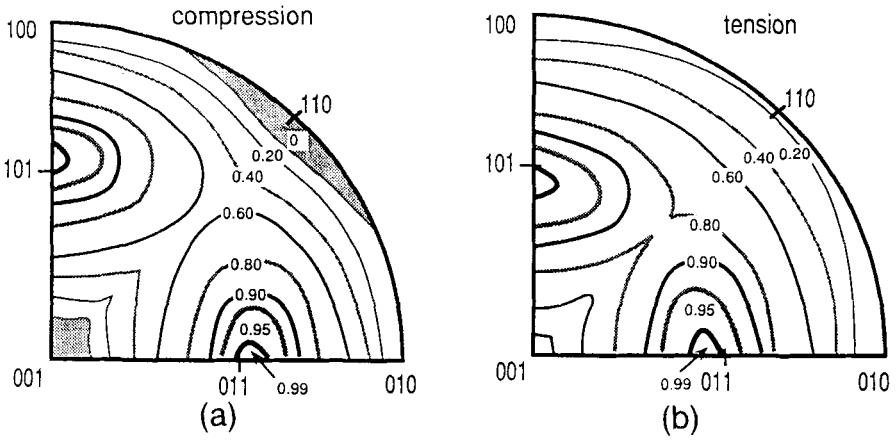

Fig. 2. Transformation stereograms for (a) compression and (b) tension. Contours are for normalized stress assistance W/W_{max} at values shown. The gray area in (a) represents orientations which receive no positive stress assistance.

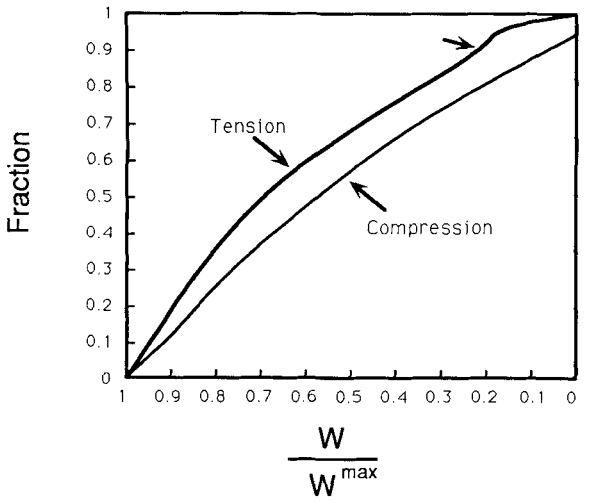

Fig. 3. Calculated fraction of grains versus normalized stress assistance. Perturbation in tension denoted by the arrow is due to the secondary component of transformation.

stress axis. In Figs. 4(a)–(d), tetragonal (001) and (100) pole distributions in compression and tension are given at various transformation fractions. (The stress assistance for those grains transformed can be read from Fig. 3.) As expected from the previous section, the first tetragonal grains to transform lie with (00l) poles approximately 45° from the stress axis in both tension and compression. The difference between tension texture and compression texture is not significant for the tetragonal phase.

In a similar fashion, the transformation pole distributions for any tetragonal $\{hkl\}$ can be predicted. This is fortunate, since the simple relationships shown for the pole distributions of Figs. 4 (a)–(d) are not of great utility, due to the relatively weak intensities of the (00*h*) and (*h*00):(0*h*0) reflections and their overlap with monoclinic reflections. The tensile pole for $\{hhh\}$, (*hh*0) and (*h*0*h*):(0*hh*), (113) and (131):(311) are of greater utility due to the larger X-ray intensities. The calculated tensile pole distributions for these poles, shown in Fig. 4(e)–(i), demonstrate that (*hh*0) and (*h*0*h*):(0*hh*) reflections should produce very strong and simple textures. For circumstances under which the entire pole distributions are readily measurable, the pole distributions of these reflections should provide the best opportunity for finding a substantial variation over the range of specimen orientations.

Pole distributions of monoclinic phase are more complicated. First, because of lower symmetry, more reflections are present. Shown in Fig. 5 are monoclinic pole distributions for $\{hhh\}$ reflections, assuming the most favorable variant selection according to the stress assistance. They are given as the following ratios:

$$m_l = \frac{|\{hhh\}_L}{|\{hhh\}_L + |\{hhh\}_S}$$

$$m_s = \frac{|\{hhh\}_S}{|\{hhh\}_S + |\{hhh\}_L} \qquad (6)$$

where m_l is the fraction of long $\{hhh\}$ monoclinic reflections, i.e., $(\bar{1}11)$, and m_s is the fraction of short $\{hhh\}$ monoclinic reflections, i.e., (111). It is evident that the two reflections have rather different distributions due to the selection of the monoclinic orientations. Furthermore, the tension texture and compression texture are very different for the monoclinic case, in contrast to the tetragonal case. This is because of the lower symmetry of the monoclinic phase—the stress axis is not usually a symmetry axis. We note further that, at the completion of transformation, the monoclinic pole distribution in a 100% monoclinic specimen is not random, unlike the tetragonal pole distribution in a 100% tetragonal specimen before any transformation. Indeed, even if we modify our assumption and allow no selection of the tetragonal orientation, the selection of the monoclinic variant alone will result in a texture for the monoclinic pole at the completion of the transformation. The latter texture is, of course, independent of the amount of transformation and should be identical to the branch shown in Fig. 5 at the completion of transformation. The tetragonal phase has no texture in such a case.

IV. Pole Distributions on the Fracture Surface

From a practical point of view, it is of interest to know the pole distribution on the fracture surface. The preparation of pole figures from tensile fracture surfaces is complicated by the surface roughness and the fact that only a thin region near the fracture surface contains substantial transformation. Thus, it is not realistic to measure the pole distribution over a range of orientations. On the other hand, we expect that different tetragonal poles should be depleted to different extents on the fracture surface, since the transforming tetragonal variants are preferentially selected in their orientations.

A fracture surface contains facets which are not always parallel to the tensile stress axis. To account for the surface roughness of the fracture surface, it seems more realistic to compute the peak intensities of the various diffracting tetragonal reflections within a certain solid angle (e.g., ± 5°) from the tensile axis. The results are shown in Fig. 6 for different amounts of transformation fractions. From Fig. 6(a) it is clear

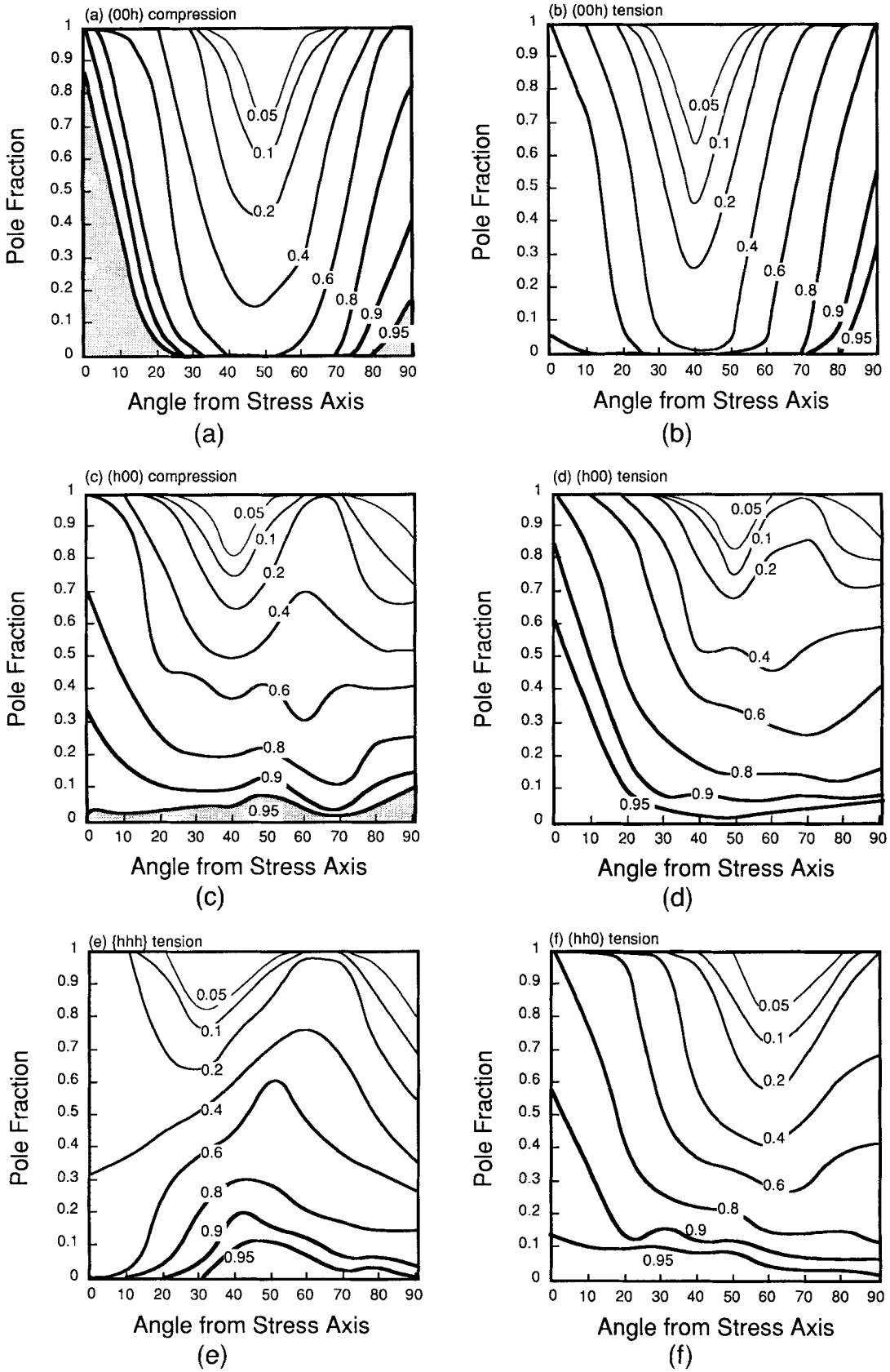

Fig. 4. Tetragonal transformation pole distributions showing pole fraction versus orientation for (a) (001) compression, (b) (001) tension, (c) (100) compression, (d) (100) tension, (e) {111} tension, (f) (110) tension, *see next page*.

that the tetragonal (202):(022) peaks should be depleted almost immediately on the tensile fracture surface, whereas the (220) and (131):(311) peaks remain strong even after most of the tetragonal grains have become monoclinic. Similar calculations for monoclinic reflections, shown in Fig. 6(b), indicate that the ($\bar{2}02$) peak should become prominent almost immediately, whereas the ($\bar{2}11$) and ($\bar{1}13$) peaks will remain weak for much of the transformation. In actual application, these sequences can be used to qualitatively compare changes in peak height ratios on the tensile fracture surface.

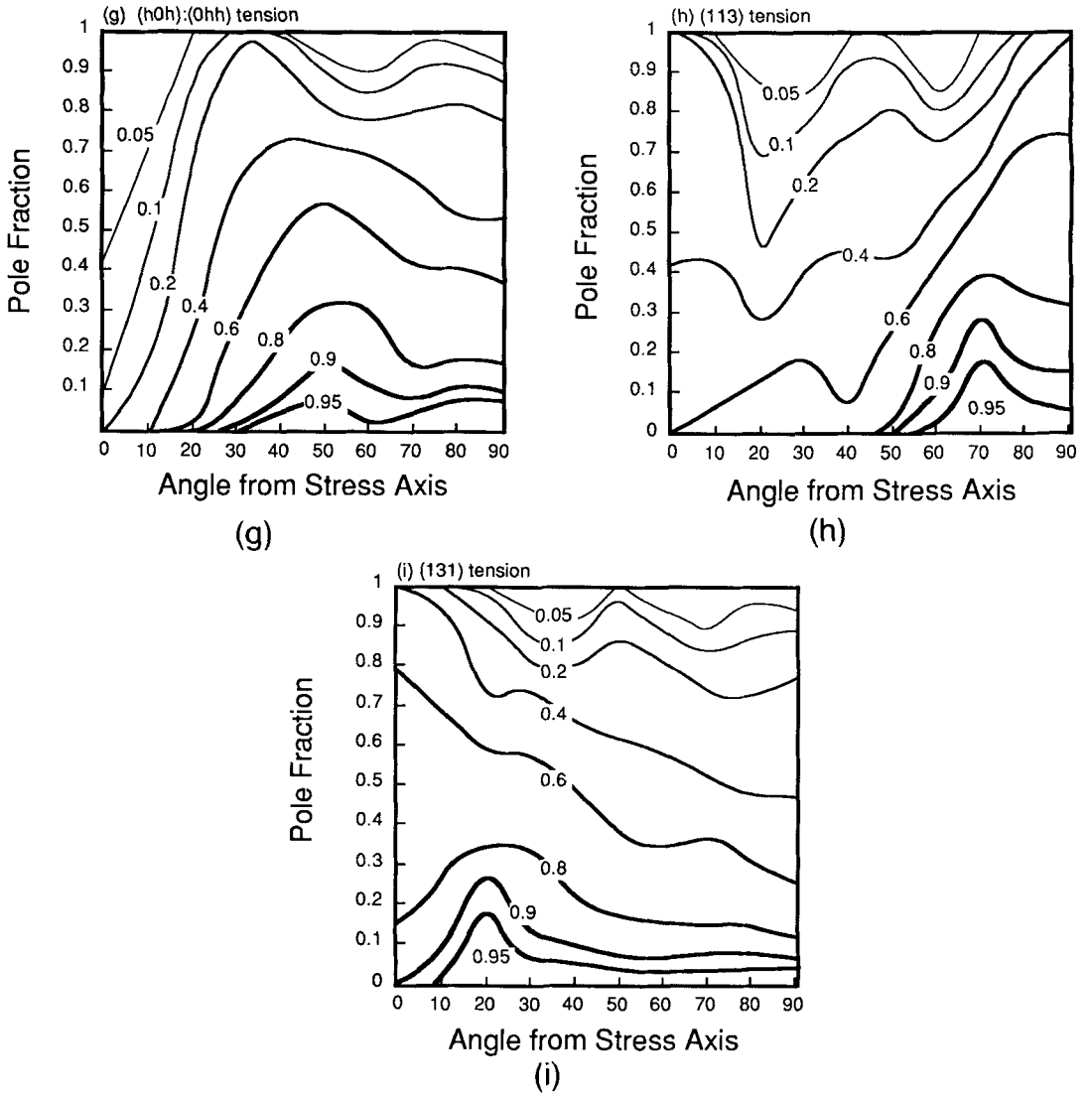

Fig. 4. (cont.) (g) (101):(011) tension, (h) (113) compression, (i) (131):(311) tension. Numbers next to curves are fractions of transformation. The gray regions indicate regions which do not transform in compression.

V. Experimental Evaluation of Transformation Textures

(1) Materials and Experimental Procedure

As shown by Reyes-Morel and Chen,[7,11,19–21] both Ce-TZP and Mg-PSZ ceramics can be deformed to significant strains via transformation plasticity. Ce-TZP is a fine-grained, all-tetragonal zirconia ceramic which can transform to near-completion. In the specimens evaluated here, transformation proceeds initially by forming transformation bands which span across many grains, indicative of autocatalysis. The stress–strain curve features a perfect plastic regime followed by strain hardening toward the latter part of transformation. Mg-PSZ is a MgO-stabilized two-phase zirconia containing cubic coarse grains with coherent tetragonal precipitates within the grains. Transformation proceeds by forming transformation bands which span across tetragonal precipitates and the cubic matrix but are usually terminated at the cubic grain boundaries. The stress–strain curve features strong strain hardening from the very beginning.

Comparisons of the measured X-ray peak intensities of various reflections on the deformed specimens readily demonstrated that they were different from those of the undeformed specimen. (The latter generally conform to the diffraction pattern of the powder specimen.) A more detailed determination of pole distributions was thus warranted to better quantify the observed texture. Pole distributions for strong X-ray reflections of the tetragonal and monoclinic zirconia phases were determined on sections of Ce-TZP specimens deformed in axisymmetric compression as described by Reyes-Morel and Chen.[7,19–21] The texture measurements in this investigation refer to those specimens designated in Table I, where the values of strains are from the previous studies. Pole distribution data were obtained from two orthogonal sections with standard corrections for specimen angle during examination in an X-ray pole figure goniometer. Cu$K\alpha$ radiation was used for all measurements.

(2) Deformation Results and Analysis

Some characteristics of the transformation process in compression experiments limit the resolution of texture. First, autocatalysis of the transformation as evidenced by the formation of shear bands overrides the variant selection consideration for the tetragonal phase, at least in the early stages of compressive deformation.[19,20] Hence, a substantial component of the initial transformation may be dominated by random selection of the tetragonal grains which lie within the shear bands. Nevertheless, most of these grains should still produce monoclinic variants with favorable stress assistance in order to generate compressive strains observed. The second difficulty is due to peak overlap between tetragonal and monoclinic grains. Since

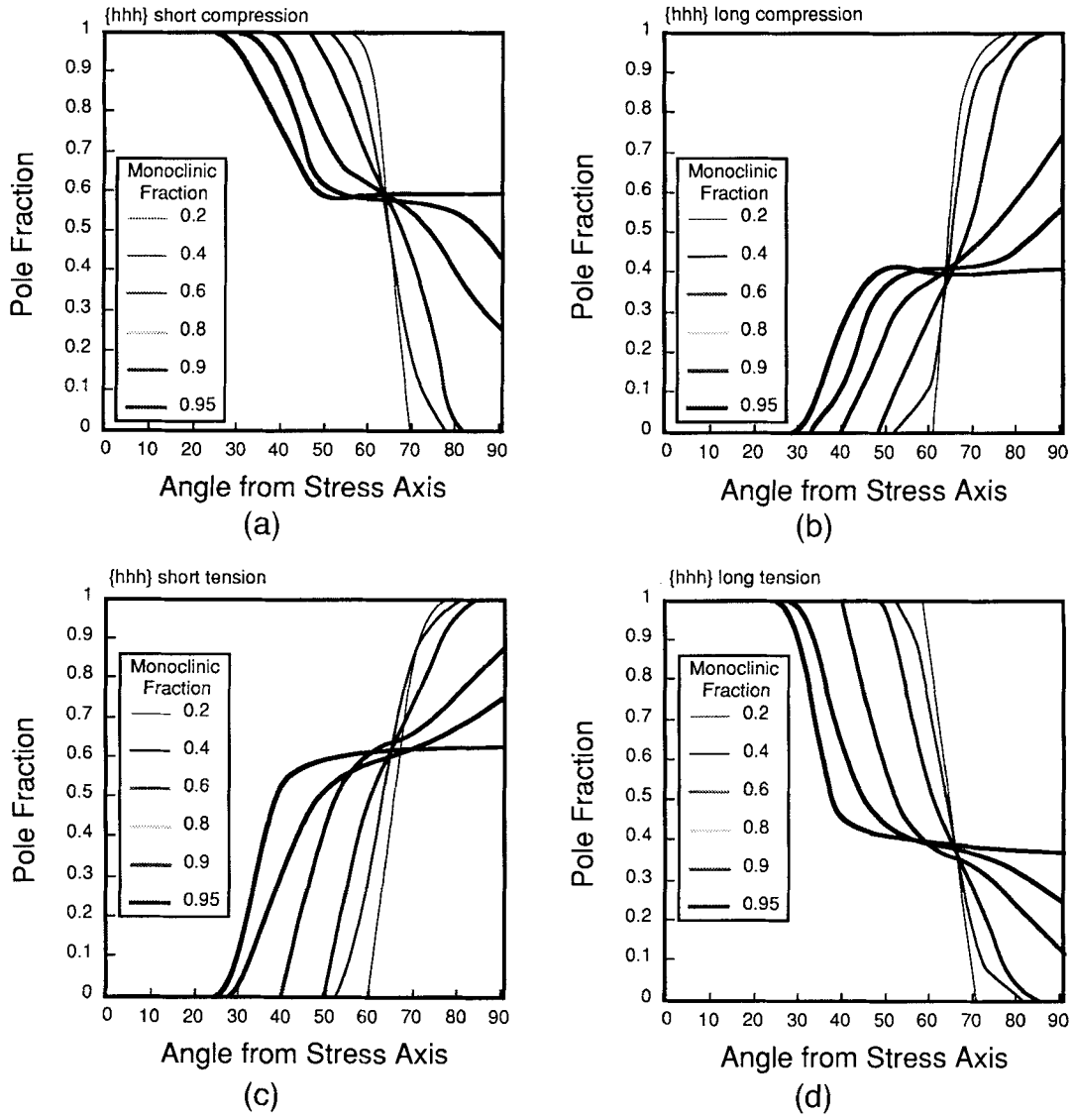

Fig. 5. Monoclinic pole fractions in (a) compression and (c) tension for {111} reflections, m_s, which have a shorter d-spacing. Also in (b) compression and (d) tension for $(\bar{1}11)$ reflections, m_l, which have a longer d-spacing.

the monoclinic phase generally has a smaller structure factor for X-ray diffraction, peak overlap is not as severe at the early stage of transformation as in the later stage. Because of these difficulties, though, demonstration of transformation texture and its comparison with the perfectly coupled, stress-assistance model should be made by noting qualitative trends of texture development and similarities in the shapes of the pole distributions between the experimental observation and model predictions. A direct coincidence of the experimental and modeling results is not possible.

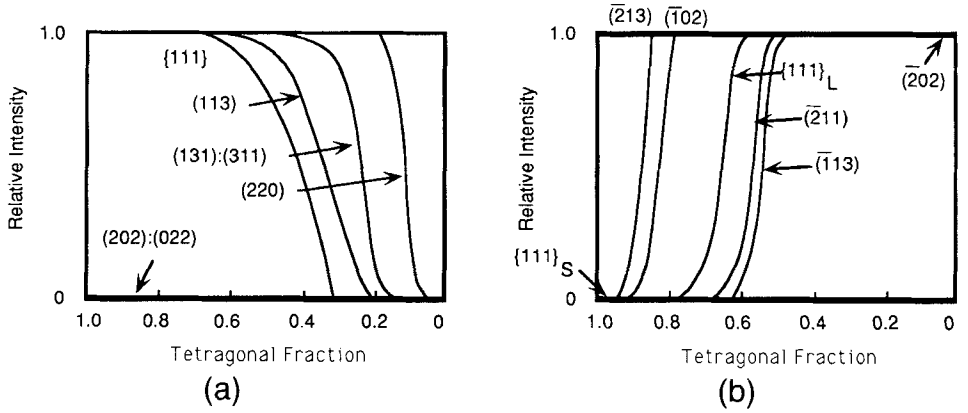

Fig. 6. Predicted (a) depletion of tetragonal reflections and (b) emergence of monoclinic reflections versus fraction of transformation. Reflections within ± 5° from the tensile axis are counted.

Table I. Strains of Deformed Zirconia Samples for Texture Measurements

		ε_{axial}	ε_{radial}	ε_{vol}
Ce-TZP	A	−0.00825	0.01085	0.01345
	B	−0.01200	0.02200	0.03200
	C	−0.02740	0.03550	0.04360
Mg-PSZ	M1	−0.00455	0.00656	0.00857
	M2	−0.00476	0.00832	0.01188
	M3	−0.00765	0.01091	0.01417

(A) Tetragonal Texture in Compression: In this section, we focus on the tetragonal texture for the {111}, {220}, and (202):(022) reflections. They were chosen because of better resolution as judged by the relative intensity and isolation from other peaks of zirconia polymorphs. According to Fig. 4, the predicted texture for the {111} pole should develop a broad peak around 40°–60° as deformation proceeds. Likewise, for the {220} pole, the pole fraction should decrease rapidly from 0° to 30° before it levels off. Finally, the (202):(022) pole fraction should have a broad peak around 50° and a shoulder at higher angles. These qualitative, though distinct, features should be most prominent and can be best compared with the experimental results at the halfway point in transformation. Pole distribution data of experimentally observed {111}, (220), and (202):(022) tetragonal reflections are plotted for Ce-TZP along with the model predictions in Fig. 7. The experimental curve labeled B has less transformation than the curve labeled C. Due to overlap between the tetragonal and monoclinic reflections, data for specimen B are given only for (220) and (202):(022) reflections. As predicted, there is a broad peak developing at around 50° in both {111} and (202):(022) pole distributions, and a rapid decrease at lower angles in the (220) pole distribution, although the observed textures are generally less pronounced than expected from the model prediction at half-transformation by assuming complete variant selection for both tetragonal and monoclinic phases.

(B) Monoclinic Texture in Compression: The measured texture of the monoclinic phase should be much more pronounced than the tetragonal texture because of the shear transformation strain which must be produced during compression even if no tetragonal variant selection is adopted. This monoclinic texture is shown in Fig. 8 for two levels of compressive strain in 12 mol% Ce-TZP. Here we compare two {111} reflections which are distinct for monoclinic phase. All the peak intensities have been first normalized by their respective structure factor, then their fraction is computed in order to compare

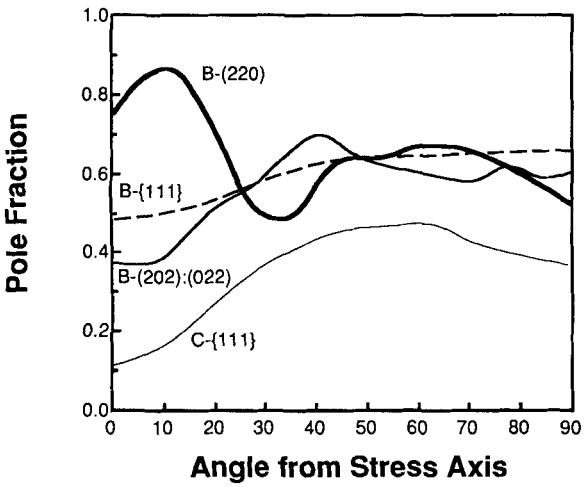

Fig. 7. Experimental data (for Ce-TZP samples B and C) for tetragonal (a) {111}, (b) (220), and (c) (202):(022) reflections.

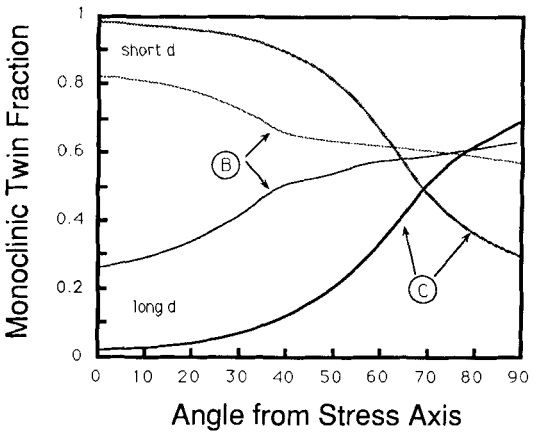

Fig. 8. Monoclinic pole fractions for the long ($\bar{1}11$) and short (111) reflections for Ce-TZP samples B and C. The pole fractions were calculated after adjusting for the smaller relative structural factor (0.65) for (111) reflection.

with the model prediction previously given in Figs. 5(a) and (b). The extreme asymmetry in favor of one variant is very dramatic at lower angles, which is consistent with the prediction of Fig. 5(a). Note that in this case the predicted texture is extremely different for tension and compression. Thus, the agreement provides direct evidence of the variant selection of monoclinic texture in accordance with the stress assistance. However, unlike the prediction of Figs. 5(a)–(b), the {111} texture becomes stronger with increasing fraction of transformation. This would be consistent with the substantial contribution of post-transformation twinning under the stress bias which becomes more dominant at later stages of deformation.

(C) Texture on Tensile Fracture Surfaces: Experimental evidence supporting the model is also apparent in X-ray examination of tensile fracture surfaces. The change in peak height ratios on the fracture surface should follow the predictions of Figs. 6(a) and (b) for the tetragonal and monoclinic phases. Specifically, if such results are presented in the form of inverse pole figures, defined as

$$P_{hkl} = \frac{I_{hkl}/I^{\circ}_{hkl}}{\frac{1}{q}\sum_{q}\frac{I_q}{I^{\circ}_q}} \tag{7}$$

where the peak intensity is first normalized by its value of powder diffraction I°_{hkl} and then by the sum of all numerators for q reflections considered in the data analysis, the P_{hkl} values thus obtained should follow the sequence of phase depletion/formation given in Fig. 6. ($P_{hkl} = 1$ for all reflections if no variant selection occurs.) Results from several X-ray measurements on fracture surfaces are given in Table II for a 12 mol% Ce-TZP broken in impact loading. Clearly, no random texture is obtained, and a strong variant selection in favor of transformation of tetragonal grains in (202):(022), {111}, (113) orientation in favor of (131):(311) and (220) orientations is evident. This relative tendency for transformation is consistent with the model prediction in Fig. 6(a), where the tetragonal reflections which are depleted most are the ones which receive the most stress assistance.

Table II. Inverse Pole Figure Values for Tetragonal Reflections on Fracture Surfaces Determined Using Eq. (7)

Tetragonal reflection	P
(202):(022)	0.8
{111}	0.8
(113)	0.8
(131):(311)	1.3
(220)	1.3

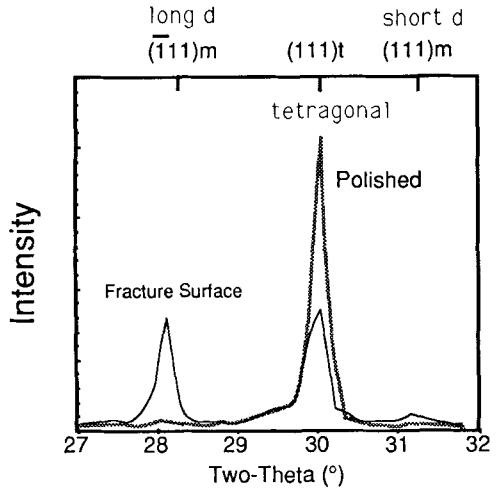

Fig. 9. X-ray diffraction of polished and fractured surfaces of 12 mol% Ce-TZP.

There is also a monoclinic texture on the fracture surface. The direct evidence is shown in Fig. 9, where the peak height ratio of $(\bar{1}11)_{long}$ and $(111)_{short}$ reflections is clearly different from that expected for monoclinic powders (ratio = 1.5). The monoclinic inverse pole figure values have been calculated and are given in Table III for the same 12 mol% Ce-TZP broken in impact. The relative values of all five integrated intensities are consistent with the prediciton of Fig. 6(b). The first monoclinic orientations to form on the fracture surface are ones with $(\bar{2}02)$ poles nearly parallel to the tensile axis. Note that although the selection of a $(\bar{1}11)_{long}$ variant in favor of $(111)_{short}$ might perhaps be attributed to the selection of a monoclinic variant alone, the appearance of the $(\bar{2}02)$ pole in favor of others must be partly due to the selection of a tetragonal variant.

(D) Transformation Plasticity: We have already tabulated in Table I the macroscopic strains of the deformed specimens undergoing transformation. The transformation strains of a macroscopic sample can be compared with the model prediction using Eq. (3), averaged over grains of all orientations. The monoclinic fraction at any point is simply the number of transformed grains (m) over the total number of grains (n) and can be directly related to the volume strain of the specimen. Shown in Fig. 10 are the axial and radial strains against the volume strains and the monoclinic fraction for Mg-PSZ and Ce-TZP, with the strains for the Mg-PSZ corrected for the volume fraction (≈0.33) of tetragonal precipitates. Also shown for comparison is the prediction for different transformation conditions: (a) both tetragonal and monoclinic variant are selected according to stress assistance, labeled as "t/m selection," and (b) random tetragonal variant but selection for monoclinic variant, labeled as "m selection." The prediction of model (a) for axial strain can be easily obtained from Fig. 3 by integrating axial strain, which is proportional to W/W_{max}, over the fraction of grains. The radial strain can then be deduced from the axial and the volumetric strains. The prediction of model (b) can be easily obtained by drawing a straight line between the origin and the endpoint of model (a).

Comparing predictions of models (a) and (b), it is clear that selection of monoclinic variants is the most important factor that produces nondilatational strain components. However, with the small differences that distinguish the two models, we are not able to definitively differentiate them, using strain data alone. This is particularly true when a small portion of the specimen strains may be attributed to microcracking.[21] Nevertheless, the direct evidence of tetragonal texture presented earlier leaves little doubt that a certain degree of tetragonal variant selection must also operate in these experiments.

Table III. Inverse Pole Figure Values for Monoclinic Reflections on Fracture Surfaces Determined Using Eq. (7)

Monoclinic reflection	P
$(\bar{2}02)$	2.4
$(\bar{2}13)$	1.7
$(\bar{1}02)$	1.4
$(\bar{1}11)$	0.6
$(\bar{2}11)$	0.6
(111)	<0.1

VI. Discussion

(1) Stress Assistance

There are several central questions in the literature of transformation plasticity and toughening which are directly relevant to the present study. These concern the relative importance of shear compared to dilatation, the significance of deformation twinning subsequent to transformation *vis a vis* variant selection during transformation of the monoclinic phase, and lastly the extent of variant selection of tetragonal and monoclinic phases and their connection to transformation/deformation strain. Our experimental observations of transformation texture in both tensile and compressive deformation, and the theoretical analysis of the stress assistance in connection with transformation texture and strains, have provided some definitive insight to these issues. These are discussed below.

First, concerning the shear contribution, the ubiquitous observation of transformation texture of the tetragonal phase in all modes of stress-induced phase transformation is a direct affirmation of its significance. Otherwise, with dilatation alone, no preference for any variant in the parent phase should arise. (Texture of the product monoclinic phase can be a result of deformation twinning, as will be discussed in the next paragraph.) In fact, some of the transformed specimens we used were not only deformed in compression but also subject to a hydrostatic pressure,[7,19-21] yet nearly full transformation could be effected under such a highly compressive stress state, in contradiction to the dilatation picture. This relative insensitivity to the hydrostatic stress state is also evident in the predicted tetragonal transformation texture which is similar in both tension and compression. Thus, we believe the issue that the shear component is predominant for transformation texture of the tetragonal phase is fully settled as far as stress assistance is concerned.

The second issue concerns the mechanism for generating the shear strain which can be either by the selection of a monoclinic variant during transformation or by deformation twinning of the transformed monoclinic phase. Both mechanisms can result in a monoclinic texture when subject to a stress bias. We believe our data are supportive of the operation of both mechanisms. For example, the prominent presence of $(\bar{2}02)$ monoclinic reflection is a direct consequence of the preferential transformation of tetragonal grains of (202):(022) orientation in the tensile stress direction. (See Tables II and III.) On the other hand, the tendency for obtaining further sharpened bias in favor of the $\{111\}_{short}$ reflection for the monoclinic phase as deformation proceeds is opposite to the expectation of variant selection during transformation but would be consistent with the deformation twinning picture. At any rate, these two contributions are likely to be coupled in view of the ready tendency for monoclinic twinning and the frequent observation of its occurrence in even macroscopically unconstrained transformation.[22]

It is probably reasonable to suggest that, while monoclinic variants are selected according to stress assistance during transformation, twinning which accommodates transformation strain to alleviate internal stresses occurs simultaneously and also subsequently after spontaneous transformation events are completed.

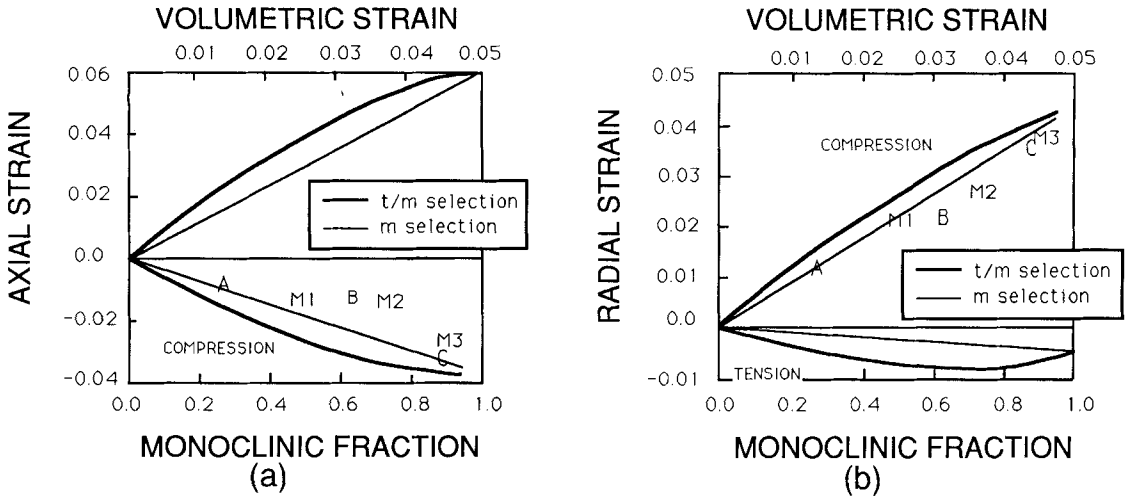

Fig. 10. (a) Axial and (b) radial strain versus volumetric strain or, equivalently, monoclinic fraction of Ce-TZP and Mg-PSZ samples. Also shown are model predictions assuming both tetragonal and monoclinic variant selection (*t/m* selection) and only monoclinic variant selection (*m* selection).

The last issue concerns the extent of tetragonal and monoclinic variant selection which dictates the partition of transformation strain under the prevailing stress state. Less than full efficiency of the selection of either the tetragonal variant or the monoclinic variant will give rise to less stress assistance and lower shear strains. This issue has more consequence in the initial stage of transformation, when the choice for variant selection is large. Although our texture study on tetragonal poles confirms the operation of tetragonal variant selection, it can only affect the strain partition in a minor way, as indicated by the model calculation shown in Fig. 10. Independently, from transformation yield stress measurements under different hydrostatic stress states, Chen and Reyes-Morel have concluded[7,11,21,23] that the initial transformation yielding reflects some but incomplete variant selection.[23] These results appear to be consistent with each other in their conclusion of the less than full efficiency of stress coupling. Finally, as the transformation proceeds to completion, the selection of tetragonal variant is of little importance to the total strain, which is entirely governed by monoclinic variant selection as shown in Fig. 10. Our experimental data shown there also indicate that the magnitude and the partition of transformation strains are very close to the model prediction at this point. Thus, even if deformation twinning can be regarded as a distinct mechanism, there seems to be no need to distinguish it as far as strain evaluation is concerned.

Overall, then, we may propose that the model for stress assistance as given by Eq. (2) provides an adequate basis for understanding stress-induced transformation mechanics, especially if it is augmented by some realistic estimate of the coupling efficiency in the beginning phase of the transformation.

(2) Implications

Several features of the pole distributions given in Figs. 4–6 have other implications on the research of zirconia transformation. One is the suggestion that preferred transformation of zirconia should leave highly distorted diffraction intensities, which, if used indiscriminately, could result in an erroneous estimation of the fraction of transformation. Note that the model predicts complete transformation of those zirconia grains with {111} normal to the tensile axis ($\alpha = 0°$) before two-thirds of all the other tetragonal grains have transformed. Considering the common use of the {111} tetragonal and monoclinic reflections to estimate the transformability of the zirconia, it is clear that any tendency for preferred transformation on the fracture surface would lead to overestimation of the fraction of transformation. Inasmuch as strain and X-ray texture data presented here have established a strong tendency for tetragonal and monoclinic variant selection in both compressive and tensile deformation of tetragonal zirconias, it seems certain that all past investigations of zirconia that relied on X-ray measurements on fracture surfaces overestimated the transformation fraction by as much as 10% to 30%. Textures produced by grinding zirconia ceramics,[9,12,13,15,17,18] which have a biaxial compressive stress in the surface, should be analogous to the case of uniaxial tension normal to the surface. Estimation of phase fraction will be liable to the same caution mentioned above.

The most intriguing suggestion of this investigation is the potential for toughening benefits by producing a tetragonal texture that maximizes tensile strain in fracture. It is noted that the monoclinic grains which are the most measurable on the fracture surface are those that produce the greatest tensile strain, whereas the tetragonal grains which produce no monoclinic {111} reflections on the fracture surface do provide a greater component of dilatant strain than shear strain. The results given in Fig. 3 indicate that a *h*0*h*:0*hh* fiber texture would produce larger transformation strains along the fiber axis. For tensile deformation, a nearly 50% increase in potential tensile strain, from 6% to 9%, would be available in such a textured material. For domain switching (tetragonal twinning), the orientation relationship is quite different.[24] Therefore, the potential for enhancing fracture toughness via processing-imparted texture seems clear. Early results suggest that this can be realized in zirconias.[25]

VII. Conclusions

The large shear component of the *t*-to-*m* transformation in zirconia causes a stress-induced preferred orientation of the tetragonal and monoclinic variants. The resultant texture has been analyzed theoretically and experimentally. The following conclusions can be drawn.

(1) The transformation texture can be understood in terms of stress assistance to transformation coupling stress and transformation strain of the appropriate tetragonal and monoclinic variants.

(2) The shear component is the dominant factor controlling the textures, as evidenced by the selection of tetragonal and monoclinic variants.

(3) In a random polycrystal, the tetragonal texture has a relatively small tension–compression asymmetry.

(4) The monoclinic texture is very pronounced and highly asymmetric in tension and in compression.

(5) On the fracture surface, the tetragonal (202):(022) peaks are first depleted, while the (220) and (131):(311) peaks remain strong. The monoclinic ($\bar{2}02$) peak emerges most

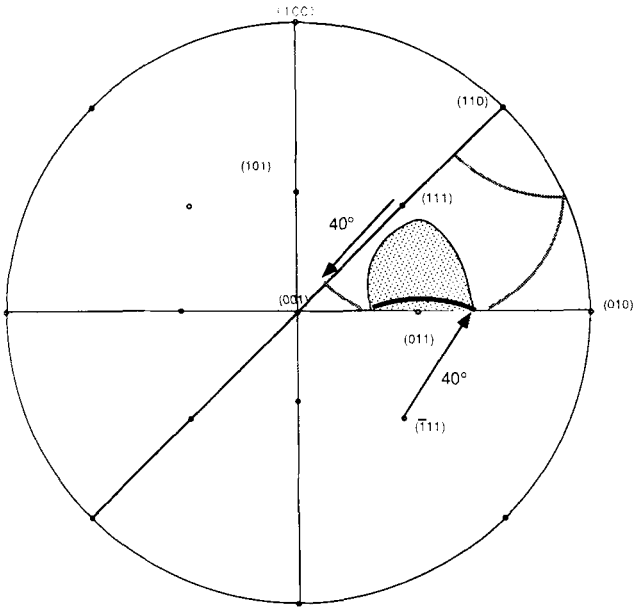

Fig. A1. A stereogram of (001) projection. In the 001:010:110 octant, the trajectories depicted are at 40° from the stress axis on a {111} pole distribution. The black portion has transformed, while the gray portion has not. (See text.)

strongly, whereas the $(\bar{2}11)$, $(\bar{1}13)$, and $(\bar{1}11)$ peaks remain weak.

(6) The above textures make it generally inadvisable to estimate phase fraction from single-peak data such as {111}. Toughness improvement may be realized by a judicious tailoring of the tetragonal texture to maximize the transformation strain in the tensile direction.

Acknowledgments: Discussion and suggestions from V. Iyer, P. Reyes-Morel, and J. S. Cherng are gratefully acknowledged.

Appendix

Figures on textures were determined using random grain orientations chosen within a stereographic octant bounded by the (00*h*), (*h*0*h*), and (*h*00) poles. After determining the values of Eq. (2), which represented specific monoclinic fractions, the stereograms and transformation pole distributions were calculated by determining the fraction of grains at a given orientation from each {*hkl*}. To illustrate the principle of such a calculation, Fig. A1 shows a schematic example at a small fraction of transformation. The trajectory represented by the gray contour consists of tetragonal orientations at 40° from the stress axis on a (111) pole distribution. The black arc is the same but on a $(\bar{1}11)$ pole distribution, which is degenerate with (111) in tetragonal symmetry. The latter also falls into the gray area, which corresponds to a stress assistance W/W_{max} no less than 0.6. Thus, at this level of stress assistance, the fraction of the transformed grains can be simply computed by the ratio of the length of the black arc to the total length of the black and the gray contours. In a similar fashion, the pole distributions of any {*hkl*} can be determined with due consideration to multiplicity and orientation for tetragonal or monoclinic poles. For strain calculations, the transformation strain tensor is matched to the orientations of grains which have transformed. In reality, rather than calculating the length ratios in spherical coordinates, as in Fig. A1, a set of 2000 random grain orientations were used to sample the stereographic octant. The stress assistance is individually computed for each orientation to determine its tendency for transformation. The fraction of orientations receiving a specified stress assistance is then evaluated to solve for the pole distributions. The result is finally plotted using an angular band of 5°.

References

[1]G. J. Davies and R. M. Bateman, "The Influence of Variant Selection on the Inheritance of Texture during Phase Transformations"; pp. 132–48 in *ICOTOM 6*, Vol. 1. The Iron and Steel Institute of Japan, Tokyo, Japan, 1981.

[2]F. Borik and R. H. Richman, "Preferred Transformation in Strain-Hardened Austenite," *Trans. Metall. Soc. AIME*, **239** [5] 675–80 (1967).

[3]H. Siemes and Ch. Hennig Michaeli, "Ore Minerals"; pp. 335–60 in *Preferred Orientation in Deformed Metals and Rocks*. Edited by H-R. Wenk. Academic Press, New York, 1985.

[4]R. A. Vandermeer and O. B. Cavin, "The Development of Texture and Its Role in Shape Memory Behavior in a Uranium Alloy"; pp. 181–90 in *ICOTOM 5*, Vol. 2. Edited by G. Gottstein and K. Lucke. Springer-Verlag, Berlin, Germany, 1978.

[5]W. P. Liu and H. J. Bunge, "Orientation Selective Martensite Transformation: The Transformation Probability Function"; pp. 327–36 in *Theoretical Methods of Texture Analysis*. Edited by H. J. Bunge. Deutsche Gesellschaft Metallkunde, Germany, 1987.

[6]J. DeVos, L. Delaey, and E. Aernoudt, "Orientation Dependence of Mechanically Induced Transformations in Copper-Base Alloys"; pp. 167–70 in *Texture of Materials 5*, Vol. 2. Edited by G. Gottstein and K. Lücke. Springer-Verlag, Berlin, FRG, 1978.

[7]P. E. Reyes-Morel, "An Experimental Study of Constitutive Relations of Transformation Plasticity in Zirconia-Based Ceramics"; Ph.D. Thesis. Department of Nuclear Engineering, Massachusetts Institute of Technology, Cambridge, MA, June, 1986.

[8]B. C. Muddle and R. H. J. Hannink, "Crystallography of the Tetragonal to Monoclinic Transformation in MgO-Partially-Stabilized Zirconia," *J. Am. Ceram. Soc.*, **69** [7] 547–55 (1986).

[9]A. V. Virkar and R. L. K. Matsumoto, "Ferroelastic Domain Switching as a Toughening Mechanism in Tetragonal Zirconia," *J. Am. Ceram. Soc.*, **69** [10] C-224–C-226 (1986).

[10]A. W. Patersen and R. Stevens, "Preferred Orientation of the Transformed Monoclinic Phase in Fracture Surfaces of Y-TZP Ceramics," *Int. J. High Technol. Ceram.*, **2** [1] 135–42 (1986).

[11]I-W. Chen and P. E. Reyes-Morel, "Transformation Plasticity and Transformation Toughening in Mg-PSZ and Ce-TZP," *Mater. Res. Soc. Symp. Proc.*, **78**, 75–88 (1987).

[12]A. V. Virkar and R. L. K. Matsumoto, "Toughening Mechanism in Tetragonal Zirconia Polycrystalline (TZP) Ceramics"; pp. 653–62 in Advances in Ceramics, Vol. 24, *Science and Technology of Zirconia III*. Edited by S. Somiya, N. Yamamoto, and H. Hanagida. American Ceramic Society, Columbus, OH, 1988.

[13]F. Reidinger and P. J. Whalen, "Texture on Ground, Fractured and Aged Y-TZP Surfaces," *Mater. Res. Soc. Symp. Proc.*, **78**, 25–33 (1987).

[14]K. J. Bowman and I-W. Chen, "Texture from Deformation of Zirconia-Containing Ceramics"; pp. 811–16 in proceedings of the 8th International Conference on Texture of Materials, Santa Fe, NM, September, 1987. Edited by J. S. Kallend and G. Guttstein. The Metallurgical Society, Warrendale, PA, 1988.

[15]B. S. Li, J-S. Cherng, K. J. Bowman, and I-W. Chen, "Domain Switching as a Toughening Mechanism in Tetragonal Zirconia," *J. Am. Ceram. Soc.*, **71** [7] C-362–C-364 (1988).

[16]P. E. Reyes-Morel, J-S. Cherng, and I-W. Chen, "Transformation Plasticity of CeO_2-Stabilized Tetragonal Zirconia Polycrystals V: Pseudoelasticity and Shape Memory Effect," *J. Am. Ceram. Soc.*, **71** [8] 648–57 (1988).

[17]R. H. J. Hannink and M. V. Swain, "Metastability of the Martensitic Transformation in a 12 mol% Ceria–Zirconia Alloy: I, Deformation and Fracture Observations," *J. Am. Ceram. Soc.*, **72** [1] 90–98 (1989).

[18]M. V. Swain and R. H. J. Hannink, "Metastability of the Martensitic Transformation in a 12 mol% Ceria–Zirconia Alloy: II, Grinding Studies," *J. Am. Ceram. Soc.*, **72** [8] 1358–64 (1989).

[19]A. V. Virkar and R. L. K. Matsumoto, "Ferroelastic Domain Switching as a Toughening Mechanism in Tetragonal Zirconia," *J. Am. Ceram. Soc.*, **69** [10] C-224–C-226 (1986).

[20]I-W. Chen and P. E. Reyes-Morel, "Transformation Plasticity of CeO_2-Stabilized Tetragonal Zirconia Polycrystals: I. Stress Assistance and Autocatalysis," *J. Am. Ceram. Soc.*, **71** [5] 343–53 (1988).

[21]P. E. Reyes-Morel and I-W. Chen, "Stress-Based Anisotropic Microcracking in Zirconia Polycrystals," *J. Am. Ceram. Soc.*, **73** [4] 1026–33 (1990).

[22]I-W. Chen and Y. H. Chiao, "Theory and Experiment of Martensitic Nucleation in ZrO_2-Containing Ceramics and Ferrous Alloys," *Acta Metall.*, **33** [10] 1827–45 (1985).

[23]I-W. Chen, "Implications of Transformation Plasticity in ZrO_2-Containing Ceramics, I. Shear and Dilatation Effects," *J. Am. Ceram. Soc.*, **69** [3] 181–89 (1986).

[24]K. J. Bowman, "Texture from Domain Switching of Tetragonal Zirconias," *J. Am. Ceram. Soc.*, **74** [10] 2690–92 (1991).

[25]V. Iyer and K. J. Bowman, unpublished work. □